Indian Journal of Pure & Applied Physics
Vol. 61, May 2023, pp. 343-354
DOI: 10.56042/ijpap.v61i5.70421

The Role of MgO Modifier on Physical, Structural, Optical and Thermoluminescence Properties of Lithium Borate Glass System

Navjeet Kaur[a], Vijeta Bhatia[b], Dinesh Kumar[b], Ritika Arora[b], Manpreet Kaur[c] & Supreet Pal Singh[b,*]

[a]Department of Physics, Mata Gujri College, Fatehgarh Sahib 140 407, India
[b]Department of Physics, Punjabi University, Patiala 147 002, India
[c]Department of Chemistry, Mata Gujri College, Fatehgarh Sahib 140 407, India

Received 12 January 2023; accepted 11 April 2023

Synthesis of lithium borate glass system was carried using the melt quenching technique with varying concentrations of magnesium followed by analysing the different characteristics such as physical, structural, optical and thermoluminescene using various techniques *eg*. X-ray diffraction (XRD), Fourier transform infrared spectroscopy (FTIR), UV-Vis spectroscopy, and Thermoluminescence (TL). The obtained XRD pattern confirmed the amorphous nature of the prepared samples. Relevant physical parameters have been evaluated to study the response of these properties with respect to magnesium content. The density and molar volume values showed that the network structure changed with increasing magnesium content. It is evident from the FTIR spectra that the network of the prepared samples predominantly contains BO_3 and BO_4 units. The UV-vis spectra confirmed a decrease in the direct and indirect band gap values with increase in MgO content. Optical parameters namely refractive index, electronic polarizability, reflection loss and dielectric constant were also calculated and found to be in good correlation with other studies. Following gamma rays irradiation with different doses, TL glow curves of prepared glasses were analysed. Deconvolution of TL glow curves was done using glow curve convolution deconvolution (GCCD) function and trapping parameters of isolated peaks *viz*. activation energy and frequency factor have been determined.

Keywords: Borate glasses; X Ray Diffraction; FTIR spectroscopy; Thermoluminescence

1 Introduction

Glasses are the amorphous materials having unique properties like high strength, thermal stability, hardness, high transparency and excellent resistance to corrosion. Recent developments in glasses have enabled the researchers to design new glass materials and explore their applications in telecommunications, solid electrolytes, solid state lasers and batteries[1]. Among oxide glasses, the borate glasses have high chemical durability, thermal stability, high transparency, excellent solubility of rare-earth ions and lower melting temperature[2]. Furthermore, the structure of borate glasses is intriguing because of the "boron anomaly phenomenon". It involves variations in the coordination number of network forming cations in the glass system, which affect the physical properties[3,4]. Due to high sensitivity to dose and human tissue equivalent property, borate glasses have been used in radiation dosimeters, photonic devices, nonlinear optics, lasers and other advance technologies. But borate glasses are hygroscopic in nature which restricts their applications. To overcome this drawback, network modifiers such as alkali metals, alkaline earth oxides and transition metals can be added to the host borate glass system[5-10]. In pure B_2O_3 glasses, generally the boron is present in B_3O_6 (boroxol rings). The inclusion of network modifiers to boron oxide (B_2O_3) affect the functional group; as a result, they shift up the active groups and boroxyl rings in the system and causes the conversion of BO_3 to BO_4[11]. The BO_4 units are responsible for creation of color centres and enhancement of the luminescence properties[12]. Among various modifiers, the lithium oxide in borate glasses improves the physical properties and stability of glass[13-16]. The addition of lithium oxide in borate glasses transfers some of the boron atoms from triangle BO_3 to tetrahedral BO_4 and creates vacancies to increase dislocation and formation of ionic bonds with oxygen atoms (NBO) required for luminescence[17-19]. Therefore, lithium borate glasses are of great interest in many technological applications such as luminescent materials, optoelectronic devices, ionic conductors

*Corresponding author:
(E-mail: spsmudahar@gmail.com; supreet_phy@pbi.ac.in)

and electro-chemical devices[6-8,17,20]. The thermoluminescence (TL) is a reliable, promising and cost effective technique which is helpful in monitoring of radiation exposure, calculating absorbed dose in radiotherapy and diagnostic radiology[21-23]. Thermoluminescence light emits from the heated material as a result of radiative recombination between the electrons released from the electron centre (that were previously trapped within the material due to irradiation) and holes from hole centres. TL spectroscopy has emerged as a crucial technique to estimate the defects and depth of traps formed inside the host lattice caused by previous exposure to radiation. For a personal dosimeter, the tissue equivalence is a significant feature to be considered for TL material. Lithium borate glass is a recommended dosimeter because it's tissue equivalent absorption coefficient is comparable to that of human tissue and it has higher sensitivity in comparison to other thermoluminescence materials[15,16]. Generally, the intensity and quality of the TL signal can be enhanced by introducing suitable modifier and dopant to the TL material because of the production of traps and defects in the glass system. Thus, magnesium oxide as a second modifier or activator can be added to lithium borate glasses in order to achieve effective luminescence for medical and industrial applications[19,24]. TL studies of B_2O_3–Li_2O glass system doped with MgO has been investigated in previous reports in which the shape and intensity of the glow curve is strongly dependent upon gamma ray dose or Li_2O concentrations[17]. Also, it is observed from literature that TL dosimetric properties of pure Li_2O-B_2O_3 have been studied by researchers without analyzing other kinetic parameters, structural and optical properties of glasses[25]. In the present work, lithium magnesium borate glasses with varying concentrations of MgO are chosen to study their structural, optical and physical properties in addition to thermoluminescence properties. The structural properties of the lithium magnesium borate glasses have been studied earlier in which the equilibrium phase for Li_2O-MgO-B_2O_3 glass matrix has been measured[26,27]. The primary objective of the present study is to investigate the feasibility of these glasses as a potential thermoluminescent dosimeter.

2 Experimental Procedures

2.1 Sample Preparation

Lithium Magnesium Borate (LMB) glasses of nominal compositions $70B_2O_3$-$(30-x)Li_2O$-xMgO, with x = 1, 3, 5, 7 and 9 mol% have been synthesized using melt-quenching technique. High purity analytical grade (99.99% purity) glass constituents boric acid H_3BO_3, lithium oxide Li_2O and magnesium oxide MgO provided by Loba-Chemie Company were used to prepare the samples. The constituents were weighed using electronic balance having high sensitivity and accuracy. The stoichiometric amount of these oxides was mixed together for two hours using an agate mortar to attain homogeneity. The mixture was transferred in alumina crucible and allowed to melt in an electrical furnace at temperature 1200 °C for duration of one hour. The mixture was stirred repeatedly during heating to obtain a bubble-free liquid and then poured into a preheated graphite mould. The glass sample was then annealed for two hours in another furnace at 400 °C to remove any residual internal strains. Finally, the furnace was switched off and the sample was left in the furnace for its cooling to room temperature. The Muffle furnaces used for the preparation of glasses are available at Material Science Research Laboratory, Department of Physics, Punjabi University Patiala. Table 1 enlists the compositions of the prepared glass samples along with their labels.

2.2 Characterization

2.2.1 Physical Parameters

Density is regarded as a significant parameter for detecting the structural modifications in the glassy network with the variation in glass composition. It is influenced by structural softening/compactness, change in co-ordination number, geometrical configuration and interstitial spaces in glass network[28,29].

The room temperature density measurements (ρ) of the synthesized glass samples were carried out using Archimedes principle where benzene was taken as an immersion liquid because of its non-absorbing nature. The density of prepared glass samples was calculated using the following equation:

Table 1 — Chemical composition of prepared lithium magnesium borate glass samples (mol %) along with their codes.

Composition (mol %)			Sample Code
B_2O_3	Li_2O	MgO	
70	29	1	LMB-1
70	27	3	LMB-2
70	25	5	LMB-3
70	23	7	LMB-4
70	21	9	LMB-5

$$\rho = \frac{x}{(x-y)} \times 0.876 \ (\mathrm{g\ cm^{-3}}) \quad \ldots (1)$$

where x is the density of glass in air, y is the density of glass in benzene and 0.876 gcm^{-3} is the room temperature density of benzene. The molar volume (V_m) of the samples was determined by the equation[30]:

$$V_m = \frac{M}{\rho} \ (\mathrm{cm^3 mol^{-1}}) \quad \ldots (2)$$

where M is the molecular weight of the glass sample.

The average boron-boron separation $\langle d_{B-B} \rangle$ in the glass matrix was calculated by following expression[31]:

$$\langle d_{B-B} \rangle = \left(\frac{V_m^b}{N_A}\right)^{1/3} \quad \ldots (3)$$

Where N_A represents Avogadro's number and V_m^b is the volume of boron atoms per mole which is given by the relation,

$$V_m^b = \frac{V_m}{2(1-X_B)} \quad \ldots (4)$$

X_B is the mole fraction.

The concentration of ions (N) in the interior of glass samples was computed using the following equation:

$$N = \frac{\text{Mole percent of dopant} \times \text{Density of glass} \times \text{Avogadro No.}}{\text{Average molecular weight of glass}} \ (\text{ions } cm^{-3}) \quad \ldots (5)$$

The other physical parameters such as inter-nuclear distance $r_i(\text{Å})$, polaron radius $r_p(\text{Å})$ and field strength (F) of dopant in the glass matrix were determined using previously calculated parameters as follows:

$$r_p(\text{Å}) = \frac{1}{2}\left(\frac{\pi}{6N}\right)^{1/3} \quad \ldots (6)$$

$$r_i(\text{Å}) = \left(\frac{1}{N}\right)^{1/3} \quad \ldots (7)$$

$$F = \frac{Z}{(r_p)^2} \quad \ldots (8)$$

To minimize the error, all the measurements were carried out at room temperature for three times. The average of three calculated values of parameters has been quoted in the study.

2.2.2 Structural Characterization

The amorphous nature of the prepared glass samples was analyzed using X-ray diffraction (XRD) measurement. Samples were crushed into powder form and exposed to $Cu_{K\alpha}$ radiations (λ=1.54 Å) with 2θ ranging from 10° to 80°on PANalytical X'Pert Pro XRD diffractometer at Panjab University, Chandigarh. The functional groups and the bonding vibrations of synthesized glass samples were characterized using FTIR spectroscopy with the help of Bruker Alpha-T spectrometer in the frequency range of 600 to 1600 cm^{-1}. To record the FTIR spectra, the solid glass samples were first grounded in an agate mortar to obtain a fine powder. Then transparent pellet of thickness 1 mm were made by pressing 10 mg of glass sample with 100 mg of potassium bromide (KBr) under pressure of 100 kg m^{-2} in a hydraulic press. Thin pellet samples were then attached to the sample holder and IR spectra were taken.

2.2.3 Optical Characterization

The diffused reflectance spectra (DRS) were used to analyse the optical properties of the prepared glasses using Shimadzu-2600 UV-Vis spectrometer within wavelength range of 200-800 nm. All the readings were taken at room temperature and the direct and indirect optical band gaps (E_g)were determined for all the prepared glass samples using Kubelka-Munk (K-M) function which is given by the following expression[32,33]:

$$F(R) = \frac{1-R^2}{2R} \quad \ldots (9)$$

Where F(R) and R represents the Kubelka-Munk function and reflectance respectively. The optical band gap was obtained using the following equation:

$$F(R)h\nu = k\left(h\nu - E_g\right)^n \quad \ldots (10)$$

Where k, hν and E_g represents the constant of proportionality, photon energy and optical band gap energy respectively. Depending upon the type of transition, the value of exponent n is taken as ½ and 2 for allowed direct and allowed indirect transition respectively. For calculating the band gap E_g, $(F(R)h\nu)^n$ was plotted as a function of hν and the value of E_g was then computed by extrapolating the slope to $[F(R)h\nu]^n = 0$[34,35]. The other optical parameters such as refractive index (n), dielectric constant (ε), reflection loss (R_L) and electronic polarizabilty (α_e) were determined using following expressions:

$$R_L = \left(\frac{n-1}{n+1}\right)^2 \quad \ldots (11)$$

$$\frac{n^2-1}{n^2+2} = 1 - \sqrt{\frac{E_g}{20}} \quad \ldots (12)$$

$$\varepsilon = n^2 \quad \ldots (13)$$

$$\alpha_e = \frac{3\,(n^2-1)}{4\pi N_A (n^2+2)} \quad \ldots (14)$$

2.2.4 Irradiation and Thermoluminescence Analysis

For irradiation, the synthesized glass samples were first grounded to fine powder and then annealed in a muffle furnace for two hours at 400 °C which removed any inherent or residual information. The samples were then allowed to cool to room temperature and exposed to different gamma doses of ^{60}Co source using Gamma chamber GC-1200, BRIT, Mumbai at Inter-University Accelerator Centre (IUAC), New Delhi, India where the efficient gamma dose rate was 2.872 kGy/hr. TL measurements were carried out on a Harshaw TLD reader (Model 3500) at Inter University Accelerator Centre, New Delhi, India. TL glow curve measurements were taken in the temperature range of 50 to 400 °C at heating rate of 5 °C/s. 5 mg of the sample was used for taking each TL measurement and different kinetic parameters were calculated from TL intensity peak.

3 Results and Discussion

3.1 XRD Analysis

The XRD pattern of prepared glass samples with varying MgO concentrations exhibit broad humps and diffused scattering without any distinct peaks as shown in Fig. 1. This confirmed that the prepared glass samples are amorphous in nature. The different concentrations of MgO show no noticeable changes in the XRD pattern.

3.2 Physical Parameters

To explore the alterations in the network of the glass matrix, determination of physical parameters is a useful method for investigating. Various physical parameters of prepared glasses with varying concentrations of MgO were calculated using the formulae mentioned earlier and the obtained values are demonstrated in Table 2. The physical parameter such as density is useful tool for observing structural compactness and structural modifications in the glass matrices. The variation of molar volume and density with increase in concentration of MgO is presented in Fig. 2. It is observed that as the concentration of MgO increased from 1 to 5 mol%, the density of the prepared samples increases monotonically from 2.368 to 2.514 g/cm^3 and then decreases from 2.514 to 2.400 g/cm^3 for samples containing 7 and 9 mol% of MgO. This reveals the composition dependence of density with MgO in the prepared glasses. The molar volume has opposite trend to density with increasing concentration of MgO. The increase in the density of glasses is attributed to replacement of lighter alkali metal oxide Li_2O (molecular weight = 29.88 g/mol) by the heavier alkaline earth metal oxide MgO (molecular weight= 40.304 g/mol). MgO acts as modifier in the prepared glass system and occupy the interstitial sites present in the glass structure[36-38]. An increase in the concentration of MgO from 1 to

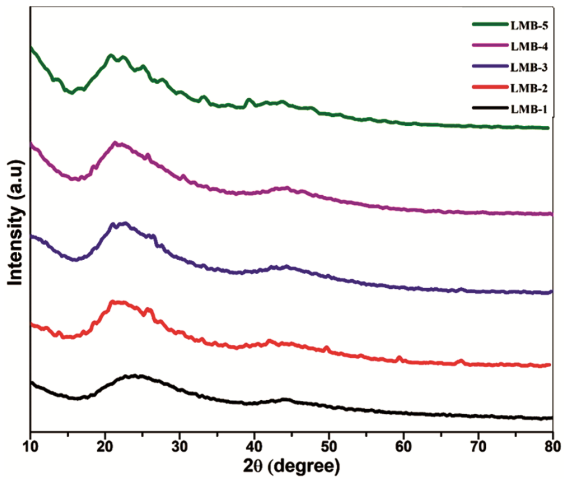

Fig. 1 — XRD patterns of prepared Lithium Magnesium Borate glasses.

Table 2 — Physical parameters of prepared glass samples

Parameters	Glass Composition				
	LMB-1	LMB-2	LMB-3	LMB-4	LMB-5
Density (ρ) (g/cm^3)	2.368	2.415	2.514	2.425	2.400
Average Mol. Weight (M) (g)	57.800	58.009	58.217	58.426	58.634
Molar Volume (V_m) (cm^3/mol)	23.325	23.020	22.058	23.222	23.614
Boron-Boron separation (<d_{B-B}>) (nm)	4.011	3.993	3.937	4.005	4.027
Volume of Boron atoms per mole (V_m^b)	38.875	38.366	36.763	38.703	39.356
Ion concentration (N×10^{22}) (ions/cm^3)	0.025	0.075	0.130	0.175	0.221
Polaron radius (r_p) (Å)	6.424	4.428	3.691	3.343	3.086
Internuclear distance (r_i) (Å)	15.940	10.990	9.162	8.299	7.667
Field strength (F×10^{16}) (cm^{-2})	0.484	1.020	1.468	1.789	2.101

5 mol% leads to a gradual increase in the bonding oxygen and oxygen-boron ratio, thereby changing the overall packing of the structural units in the fabricated glass[39]. Thus, increase in density and decrease in molar volume upto 5 mol% concentration of MgO is owed to the structural transformation of $(BO_3)_3^-$ trigonal units to BO_4^- tetrahedral units[40,41]. Further, decrease in density and increase of molar volume of glasses having MgO content 5 to 9 mol% is due to lower cross-linking and breakage of covalent bonds between boron and oxygen within the glass structure[42]. The effect of MgO as modifier and intermediate oxides can be related to the fluctuation from the linearity in density and molar volume of the prepared glasses[43]. The sample containing 5 mol% of MgO has most compact structure among all the prepared glasses. Table 2 also reports other physical parameters namely boron-boron separation, volume of boron atoms, ion concentration, polaron radius and internuclear distance of lithium magnesium borate glasses. The ionic concentration increases with the increase in concentration of MgO. Polaron radius and inter-nuclear distances decreases due to the rise in the value of ion concentration ofMg^{2+} ions. Sample LMB-5 illustrates the maximum ionic concentration with the minimum internuclear distance and polaron radius. The decrease in polar radius ascribes an increase in the compactness of the boron network of the as-prepared glass samples and supports the density and molar volume results. The average boron-boron separation and volume of boron atoms per mole shows the opposite trend as that of density. Moreover, rise in concentration of magnesium strengthens the oxygen bond strength that results in the production of strong field strength (F) around Mg^{2+} ions.

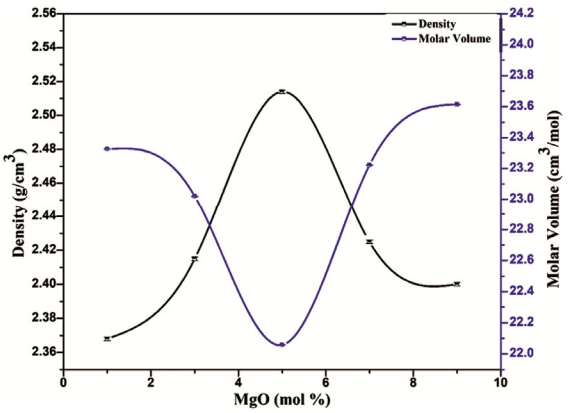

Fig. 2 — Variation of Density and Molar volume of prepared lithium magnesium borate glass samples.

3.3 FTIR Spectroscopy Analysis

FTIR spectra give the characteristic information regarding the various structural units available in the glass matrix. In the wavenumber range of 600-1600 cm^{-1}, the FTIR spectra of the prepared glasses reveals numerous vibrational bands as shown in Fig. 3. It demonstrates the existence of various functional groups in the glass, as well as the formation of tetrahedral BO_4 units. For the detailed analysis of peaks, the band positions along with their band assignments have been listed in Table 3.The prepared glasses vibrational modes are divided into three separate frequency ranges. Asymmetric stretching relaxation of trigonal BO_3 units is observed in the band region of 1200-1600 cm^{-1}. The stretching vibration of tetrahedral BO_4 structural units has been

Table 3 — Band assignment of prepared lithium magnesium borate glass samples

Wave number (cm^{-1})					Band Assignment	References
LMB-1	LMB-2	LMB-3	LMB-4	LMB-5		
683	681	694	683	689	B-O-B linkage bending vibrations	57
912	912	912	910	910	Stretching vibrations of B-O bonds in BO_4 units from tri, tetra, and penta borate groups	58
1257	1265	1267	1271	1269	B-O bond stretching in BO_4 structural units from diborate group	59
1345	1412	1414	1412	1414	Presence of pyroborate, orthoborate groups containing BO^{3-} and asymmetric bending relaxation of trigonal BO_3 units	60
1460	1460	1460	1460	1460	B-O symmetric stretching vibrations of varied borate groups in BO_3 units	61-63
1513	1519	1519	1519	1519	Anti-symmetric stretching vibrations with three NBO's of B-O-B group	64

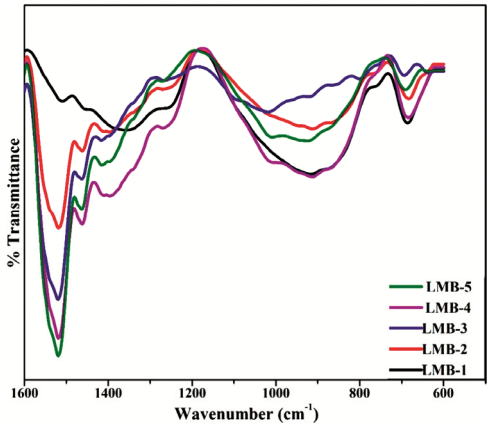

Fig. 3 — FTIR Spectra of synthesized glass samples.

linked to the IR absorption region 800-1200 cm^{-1}. The addition of magnesium ions causes an increase or decrease in the intensity of BO_3 groups, as well as a shift of the meta-centre towards a lower or higher wave number in the present glass composition. A noticeable shift of 683 cm^{-1} band is observed with change in concentration of MgO. With increase in MgO concentration from 5 to 9 mol%, a band which appeared around 912 cm^{-1} corresponds to stretching vibration of B-O bonds in BO_4 units is shifted to 910 cm^{-1}.The shift towards higher wavenumber side is also observed for 1257 and 1345cm^{-1} bands. The B–O stretching vibration of BO_3 in pyroborate, penta borate and ortho borate groups is attributed to the observed bands around 1460 and 1513 cm^{-1}. In all samples, no additional bands are observed with increasing concentration of MgO, indicating that the presence of magnesium ions does not have a major effect on the structure of borate glasses. The increase in intensity of bands can be related to the conversion of BO_3 units to BO_4 units (boron anomaly) and compactness of the structure. All the glass samples indicate the formation of BO_3 and BO_4 units fromB_2O_3. FTIR results are also in correlation with the density and molar volume results where transformation of trigonal BO_3 units into more stable and rigid tetrahedral BO_4 units raised the density and stability of the prepared glass system and leads to the decrease of molar volume.

3.4 Optical Properties (UV-Vis Spectroscopy)

To calculate the direct and indirect band gap, which gives insights about the semiconducting nature of glasses, the UV-Vis spectroscopy technique has been used. When a glass sample is subjected to UV photons, electron excitation occurs that results in the formation of strong absorption bands and the

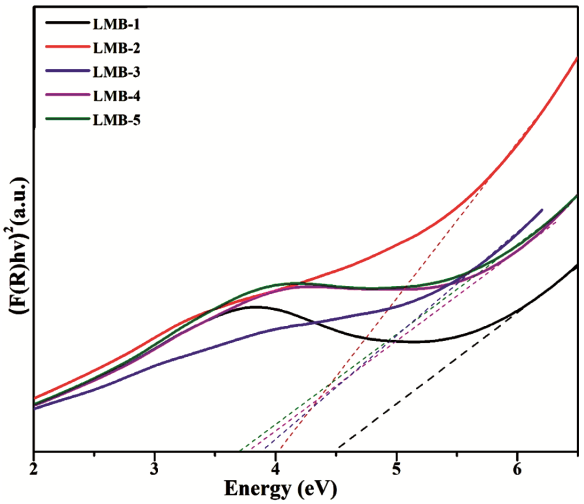

Fig. 4 — Tauc plot (Direct band gap) of lithium borate glasses with different concentration of MgO.

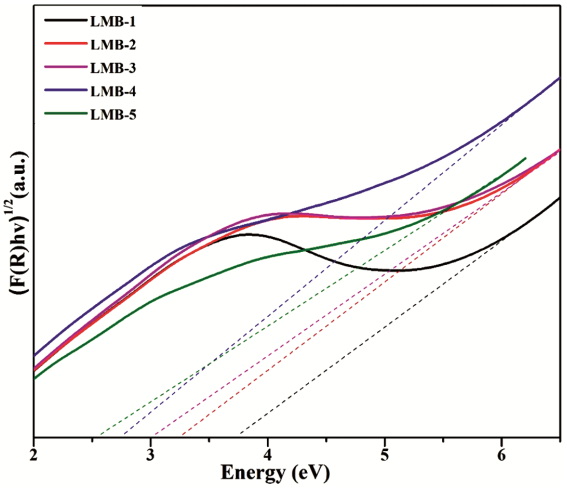

Fig. 5 — Tauc plot (Indirect band gap) of lithium borate glasses with different concentration of MgO.

appearance of opaque glasses in UV region. The graphs representing $(F(R)h\nu)^2$ and $(F(R)h\nu)^{1/2}$ as a function of photon energy $h\nu$ (known as Tau's plots) are presented in Figs. 4 & 5 respectively and the calculated values of direct and indirect optical band gap energies are listed in Table 4. Glass is a multi-element system in which different cations act together and are responsible for an increase or decrease in the band gap[42]. Increase in MgO content from 1 to 9 mol% lowered the direct and indirect energy band gap values as seen from the Table 4. The obtained direct and indirect band gap energy values occurred in the range of 4.484-3.710eV and 3.719-2.536eV respectively and their variation with respect to MgO concentration is shown in Fig. 6. For all the glass samples, direct band gap energy values are greater

Table 4 — Optical parameters of prepared Glass compositions

Optical Parameters	Glass Composition				
	LMB-1	LMB-2	LMB-3	LMB-4	LMB-5
Indirect band gap (eV)	3.719	3.254	3.015	2.747	2.536
Direct band gap (eV)	4.484	4.019	3.893	3.781	3.710
Refractive Index (n)	1.910	1.975	2.074	2.112	2.253
Dielectric constant (ε)	3.648	3.900	4.301	4.460	5.076
Reflection Loss (R_L)	0.097	0.107	0.122	0.127	0.148
Electronic Polarizability ($\times 10^{-25}$)	1.858	1.948	2.077	2.123	2.283
Optical Dielectric constant	2.648	2.900	3.301	3.460	4.076

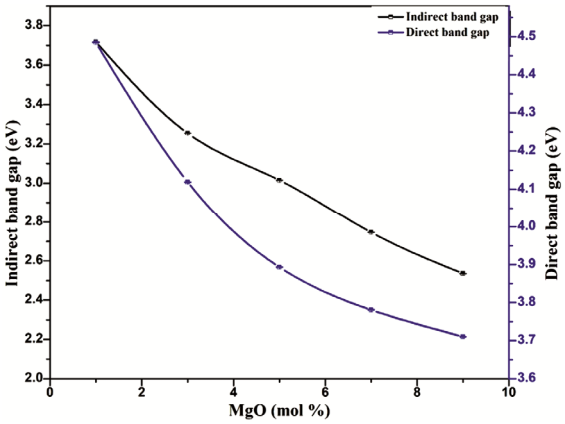

Fig. 6 — Variation of Indirect and Direct band gap of prepared glasses.

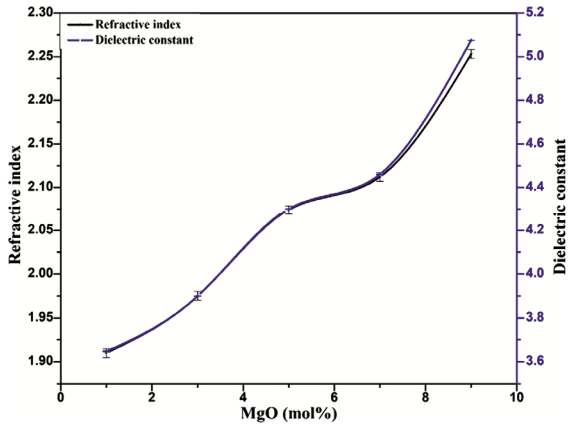

Fig. 7 — Variation of Refractive index and dielectric constant of prepared lithium magnesium borate glass samples

than the indirect band gap energy values. The role of the glass modifier is to create non-bridging oxygens by preventing normal bonding between glass-forming elements and oxygen, thereby lowering the strong bonding within the glass[44]. As the content of MgO is increased, the number of NBOs increased and the top of valence band also shifted which leads to decrease in the band gap[42]. Furthermore, decrease in the band gap energies are attributed due to the structural alterations within the network. The addition of MgO content into the glass matrix results in increment in the degree of electrons localization which leads to formation of donor centres within the glass system. The observed decrease in optical band gap energies is ascribed to the generation of these donor centres[45-47]. The indirect band gap energy values have been used to calculate other optical parameters such as reflection loss, refractive index, dielectric constant, optical dielectric constant and electronic polarizability of the glasses and these parameters are displayed in Table 4. The variation of dielectric constant and refractive index with varying concentration of MgO have also been shown in Fig. 7, which clearly indicates that refractive index increased gradually from 1.910 to 2.253 with the increase in concentration of MgO from 1 to 9 mol%. The increase in refractive index is ascribed to the creation of interstitial spaces with non-bridging oxygen atoms due to the functioning of modifier Mg^{2+} in the present network system. The dielectric constant and reflection loss of the glasses shows a similar trend as that of refractive index which may be due to the fact that magnesium ions increase the amount of non-bridging oxygen content with higher polarizability. This factor is also responsible for increment in electronic polarizability because the non-bridging oxygen's have more tendencies to polarize the bridging oxygen[48].

3.5 Thermoluminescence Analysis

3.5.1 TL Glow Curves

Figures 8 & 9 illustrates the characteristic TL glow curves of lithium magnesium borate glasses obtained upon gamma exposure of 5kGy and 10 kGy respectively when heating rate was maintained constant at 5°C/s. While analysing the TL curves, two well separated emission peaks are observed for the prepared glass samples. For 5 kGy, two peaks are observed at temperature 442 K and 570 K while for 10 kGy irradiated samples, the TL emission glow peaks are observed at temperature ranges 438 K and

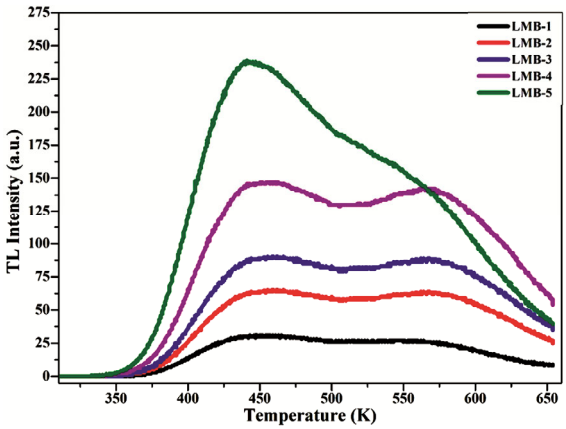

Fig. 8 — TL Glow curve for lithium magnesium borate glass system (Irradiated dose: 5 kGy)

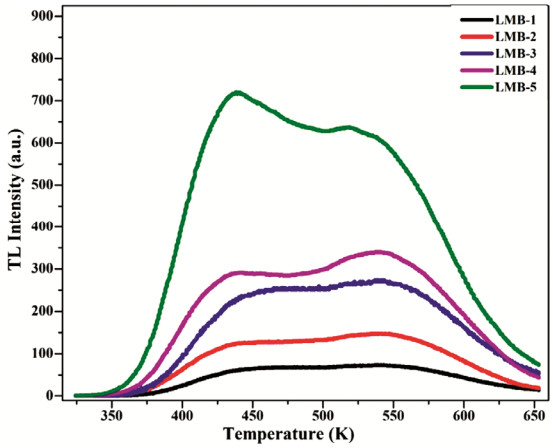

Fig. 9 — TL Glow curve for lithium magnesium borate glass system (Irradiated dose: 10 kGy)

542 K. This shows that nature of trap levels exist in a direct relationship with intensity of temperature peak i.e. low and high temperature peak were obtained with shallow and deep trap levels respectively. The shape of the TL glow curves is not influenced by variation in MgO content but TL intensity of glow peaks changes with increase in MgO concentration. Upon irradiation, the divalent magnesium ions (Mg^{2+}) interacts with gamma rays producing hole trapping centres (Mg^{3+}) and secondary electrons with excess energy. Depending upon their energy, these electrons may traverse in the glass network and the components of the glass can interact with Mg^{2+} to produce electron trapping centre. Both electron and hole trapping centres are known as color centres and localized at different energy states in the forbidden band gap region of the glass system. With an increase in the concentration of magnesium, the number of electron and hole trapping centres increase. When the irradiated samples are heated from the room

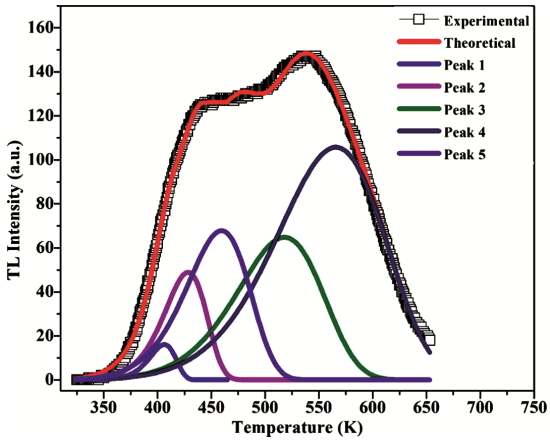

Fig. 10 — Deconvolution of TL glow curve of LMB-4 glass sample for irradiation dose 5kGy

temperature to 400 °C, the holes and electrons releases from the trapping centres and recombine with each other which enhances the TL signal[49]. Thus, Mg^{2+} plays a vital role to generate large number of trap centers and to produce TL glow curve. In current investigation, comparative increase in TL intensity was documented w.r.t. dose of irradiation (5 kGy and 10 kGy). The higher TL intensity at higher dose was owing to the increase in probability of recombination of excited electrons with holes.

3.5.2 Analysis of TL glow curves using GCCD and Calculation of trapping parameters

The observed TL glow curves of glass samples consist of two glow peaks. The observed glow curve indicates that the glass samples may not consist of just these two peaks rather these peaks can be the result of superposition of multiple peaks. Therefore, to obtain the number of isolated peaks and to extract the information of traps, experimental TL glow curves have been deconvoluted using Glow curve convolution deconvolution (GCCD) function. The least square fitting approach developed by Kitis's function was applied to deconvolute the obtained TL glow curves[50]. The isolated TL glow peaks contain information regarding the different trapping levels present in the forbidden gap of the material. Several trapping parameters viz. activation energy, geometric factor, frequency factor and order of kinetics are associated with these trapping levels that describe the nature and depth of trapping centers responsible for the TL emission. These kinetic parameters also signify the dosimetric features of any TL material. Figs. 10 & 11 display the experimentally obtained glow curves deconvoluted into isolated peaks for LMB-4 glass sample exposed to gamma dose of

Table 5 — Kinetic parameters of the prepared glass samples using GCCD method at 5 kGy dose

Sample Label	Peak No	Peak T_m(K)	$\delta = T_2 - T_m$	$\omega = T_2 - T_1$	Activation Energy E (eV)	Frequency factor $s(s^{-1})$	Geometric factor (μ_g)	Figure of Merit (FOM%)
	Peak 1	422	19	46	0.87	$5.47X10^9$	0.41	1.63
LMB-1	Peak 2	445	28	58	0.66	$1.01X10^7$	0.48	
	Peak 3	468	38	87	0.62	$3.68X10^6$	0.44	
	Peak 4	532	56	126	0.50	$2.13X10^3$	0.44	
	Peak 5	578	28	66	0.51	$6.08X10^3$	0.42	
	Peak 1	408	15	32	1.03	$3.82X10^{13}$	0.47	1.72
LMB-2	Peak 2	432	21	47	0.75	$1.61X10^8$	0.45	
	Peak 3	465	32	75	0.63	$1.08X10^6$	0.43	
	Peak 4	521	37	88	0.51	$4.79X10^3$	0.42	
	Peak 5	576	54	123	0.53	$1.36X10^4$	0.44	
	Peak 1	423	18	45	0.91	$8.82X10^{10}$	0.40	1.87
LMB-3	Peak 2	446	25	59	0.75	$1.72X10^8$	0.42	
	Peak 3	475	39	86	0.56	$1.18X10^5$	0.45	
	Peak 4	536	53	123	0.55	$7.91X10^4$	0.43	
	Peak 5	582	35	80	0.50	$2.38X10^3$	0.44	
	Peak 1	406	13	30	1.13	$4.59X10^{13}$	0.43	1.65
LMB-4	Peak 2	428	20	47	0.77	$2.98X10^8$	0.43	
	Peak 3	460	30	71	0.58	$3.79X10^5$	0.42	
	Peak 4	518	30	71	0.54	$2.18X10^4$	0.42	
	Peak 5	566	53	119	0.50	$2.66X10^3$	0.44	
	Peak 1	412	22	53	0.89	$7.77X10^{10}$	0.42	2.10
LMB-5	Peak 2	438	31	68	0.74	$1.13X10^8$	0.46	
	Peak 3	465	40	91	0.64	$9.09X10^6$	0.44	
	Peak 4	523	55	127	0.54	$2.51X10^4$	0.43	
	Peak 5	571	17	37	0.51	$7.04X10^3$	0.46	

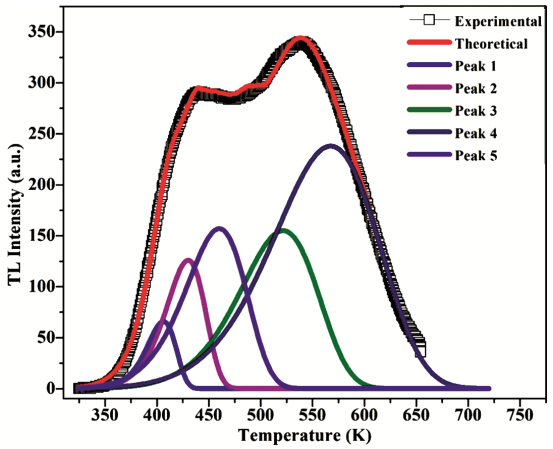

Fig. 11 — Deconvolution of TL glow curve of LMB-4 glass sample for irradiation dose 10 kGy

5 kGy and 10 kGy respectively.The accuracy of deconvolution process and quality of TL glow curve fitting is defined by the parameter called Figure of Merit (FOM) which is given by the following relation[50-53].

$$\text{FOM}\,[\%] = \frac{\sum_i |y_{i(\text{Exp.})} - y_{i(\text{Fit})}|}{\sum_i y_{i(\text{Fit})}} \times 100\% \qquad \ldots (15)$$

Where $y_{i(\text{Exp.})}$ are the experimental data points of TL glow curve and $y_{i(\text{Fit})}$ represents the respective data points of theoretically fitted TL glow curve using GCCD function.If FOM value lies below 5%, the experimental data curve is supposed to be better fit with theoretically generated curve. Glow curves having FOM value greater than 5% need to be investigated again to obtain better fit. The calculated FOM values for glow curves of all prepared compositions are below 3% suggesting that there is good agreement between experimental and theoretical fittted curve. The kinetic parameters for isolated peaks of all glow curves at 5 kGy and 10 kGy are calculated and listed in Table 5 & 6 respectively. It is observed that each isolated peak has its own trapping parameters which reveal different nature of different traps i.e. there are several deep and shallow traps present in the material. The competition among these shallow and deep traps is responsible for different releasing probabilities of charge carriers[54-56].

3.5.3 TL Fading

A TL material is considered as stable if its TL signal doesn't fade upon its storage for few days after exposure to radiation and such material can be used for dosimetry applications. The stability of TL signal of prepared samples was assessed over time period of one month. The glass sample LMB-1 irradiated with gamma dose of 10 kGy was kept at room temperature for one month without its shielding from light and

Table 6 — Kinetic parameters of the prepared glass samples using GCCD method at 10 kGy dose

Sample Label	Peak No	Peak T_m(K)	$\delta = T_2 - T_m$	$\omega = T_2 - T_1$	Activation Energy E (eV)	Frequency factor $s(s^{-1})$	Geometric factor (μ_g)	Figure of Merit (FOM%)
	Peak 1	420	19	45	0.81	$1.47X10^{9}$	0.42	2.08
LMB-1	Peak 2	449	30	53	0.77	$1.01X10^{8}$	0.55	
	Peak 3	481	28	65	0.71	$5.08X10^{6}$	0.43	
	Peak 4	531	39	89	0.60	$9.68X10^{4}$	0.44	
	Peak 5	576	55	122	0.50	$2.13X10^{4}$	0.45	
	Peak 1	418	20	46	0.78	$5.69X10^{10}$	0.43	1.67
LMB-2	Peak 2	445	26	52	0.75	$1.98X10^{8}$	0.50	
	Peak 3	476	28	66	0.68	$2.79X10^{6}$	0.42	
	Peak 4	528	34	83	0.59	$3.18X10^{5}$	0.41	
	Peak 5	578	54	123	0.50	$2.66X10^{3}$	0.44	
	Peak 1	424	19	46	0.77	$3.82X10^{8}$	0.41	1.84
LMB-3	Peak 2	454	24	57	0.71	$1.61X10^{7}$	0.42	
	Peak 3	489	35	80	0.58	$1.36X10^{5}$	0.44	
	Peak 4	545	38	87	0.65	$1.08X10^{6}$	0.44	
	Peak 5	584	56	127	0.50	$1.79X10^{3}$	0.44	
	Peak 1	406	14	33	0.98	$5.37X10^{11}$	0.42	1.96
LMB-4	Peak 2	430	20	46	0.81	$8.39X10^{8}$	0.43	
	Peak 3	460	32	73	0.59	$4.86X10^{5}$	0.44	
	Peak 4	522	39	89	0.58	$5.06X10^{4}$	0.44	
	Peak 5	568	54	122	0.50	$2.54X10^{3}$	0.44	
	Peak 1	407	16	37	0.95	$2.04X10^{11}$	0.43	2.39
LMB-5	Peak 2	432	21	51	0.73	$7.77X10^{7}$	0.41	
	Peak 3	466	29	67	0.63	$1.13X10^{6}$	0.43	
	Peak 4	521	40	91	0.57	$4.09X10^{4}$	0.44	
	Peak 5	568	54	121	0.50	$2.51X10^{3}$	0.45	

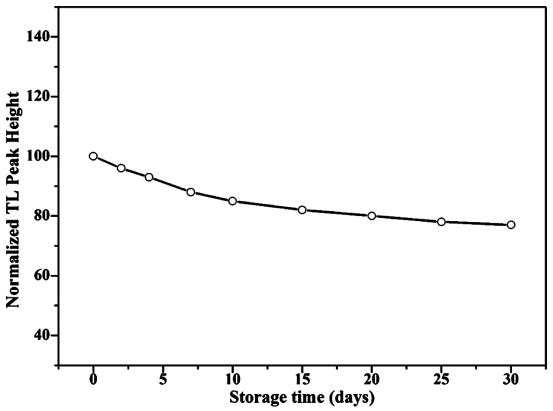

Fig. 12 — Fading curve of 10 kGy irradiated LMB-1 sample

other environmental conditions. Thereafter, the TL intensity was measured and manifests a decrease in TL peak intensity. This decrease in TL signal is due to the reduction in the number of charge carriers from the traps and provides the extent of fading in the sample. The fading curve of 10 kGy gamma irradiated LMB-1 sample is presented in Fig. 12. It shows that there is about 12% fading during first seven days. About 18% loss of TL signal is observed over 15 days of storage time and total 23% fading is calculated for the sample upon its storage for one month.

4 Conclusions

The series of lithium borate glasses with varying concentration of magnesium oxide have been synthesized by melt quenching method. The absence of sharp peaks and presence of broad humps confirmed the amorphous nature of glasses. The density and molar volume data provided further insight into glass structure and showed an irregular trend due to modifications in geometrical configuration of the glasses. The physical parameters such as polaron radius, ionic concentration, boron-boron separation and inter-nuclear distance have also been calculated and found to be in correlation with density and molar volume results. The optical band gap values were found to decrease with increasing MgO concentration due to the formation of non-bridging oxygens (NBO's). The FTIR spectra showed numerous vibrational bands and functional groups in the glass matrix which is in accordance with the density results *i.e.* formation of BO_4 units at the cost of BO_3 units. Analysing TL glow curves of the prepared glasses, two prominent peaks for gamma doses of 5 kGy and 10 kGy were observed. It is evident that magnesium ions were responsible for the

increase in glow curve intensity. GCCD method was applied to evaluate the kinetic parameters, which were found to vary with MgO content. The fading of TL signals was examined over a storage period of one month which exhibited a decrease of 23% in TL intensity. The results obtained for the present investigation suggested that the prepared glass samples are suitable for the dosimetry applications.

Acknowledgements

The authors are grateful to Inter University Accelerator Centre (IUAC), New Delhi, India for providing gamma irradiation and TL facility under project number BTR-64113.The authors would like to express sincere gratitude towards Mr. Birendra Singh, Inter University Accelerator Centre (IUAC), New Delhi, India for his valuable inputs and support in TL measurements.

References

1 Ramteke D, Swart H & Gedam R, *J Rare Earths*, 35 (2017) 480.
2 Anishia S, Jose M, Annalakshmi O & Ramasamy V, *J Lumin*, 131 (2011) 2492.
3 Varshneya A K, Fundamentals of inorganic glasses, Academic Press, New York, (2013) 106.
4 Shelby J E, Introduction to glass science and technology, Royal Society of Chemistry, United Kingdom, (2005) 76.
5 Kirdsiri K, Ramakrishna R R, Damdee B, Kim H, Kaewjaeng S, Kothan S & Kaewkhao J, *J Alloys Compd*, 749 (2018) 197.
6 Arunkumar S & Marimuthu K, *J Lumin*, 139 (2013) 6.
7 Shamshad L, Rooh G, Kirdsiri K, Srisittipokakun N, Damdee B, Kim H & Kaewkhao J, *Opt Mater*, 64 (2017) 268.
8 Zaman F, Rooh G, Srisittipokakun N, Kim H, Kaewnuam E, Meejitpaisan P & Kaewkhao J, *Radiat Phys Chem*, 130 (2017) 158.
9 Kumar K U, Babu S S, Rao C S & Jayasankar C, *Opt Commun*, 284 (2011) 2909.
10 Yuan S X, Hao X Z & Ping Z J, *Opt Mater*, 50 (2015) 110.
11 Jorgensen C K & Judd B, *Mol Phys*, 8 (1964) 281.
12 Konijnendijk W L & Stevels J M, *J Non-Cryst Solids*, 18 (1975) 307.
13 Hashim S, Mhareb M, Ghoshal S, Alajerami Y, Bradley D, Saripan M, Tamchek N & Alzimami K, *Radiat Phys Chem*, 116 (2015) 138.
14 Lakshmikantha R, Rajaramakrishna R, Anavekar R & Ayachit N, *Mater Chem Phys*, 133 (2012) 249.
15 Furetta C, Prokic M, Salamon R, Prokic V & Kitis G, *Nucl Instrum Meth Phys Res A: Accel Spectrom Detect Assoc Equip*, 456 (2001) 411.
16 Prokic M, *Radiat Meas*, 33 (2001) 393.
17 Elkholy M, *J Lumin*, 130 (2010) 1880.
18 Alajerami Y S M, Hashim S, Hassan W M S W, Ramli A T & Kasim A, *Physica B Condens Matter*, 407 (2012) 2398.
19 Mhareb M, Hashim S, Ghoshal S, Alajerami Y, Saleh M, Dawaud R, Razak N & Azizan S, *Opt Mater*, 37 (2014) 391.
20 Bhogi A, Kumar R V & Kistaiah P, *J Non-Cryst Solids*, 426 (2015) 47.
21 Liu L, Zhang Y, Hao J, Li C, Tang Q, Zhang C & Su Q, *Mater Lett*, 60 (2006) 639.
22 Li J, Hao J, Li C, Zhang C, Tang Q, Zhang Y, Su Q & Wang S, *Radiat Meas*, 39 (2005) 229.
23 Saidu A, Wagiran H, Saeed M, Obayes H, Bala A & Usman F, *Radiat Phys Chem*, 144 (2018) 413.
24 Hashim S, Mhareb M, Ghoshal S, Alajerami Y, Saripan M & Bradley D, *Radiat Phys Chem*, 137 (2017) 45.
25 El-Adawy A, Khaled N, El-Sersy A, Hussein A & Donya H, *Appl Radiat Isot*, 68 (2010) 1132.
26 Wu L, Chen X, Tu Q, He M, Zhang Y & Xu Y, *J Alloys Compd*, 333 (2002) 154.
27 Bazarova Z G, Nepomnyashchikh A, Kozlov A, Bogdan-Kurilo V, Bazarov B, Subanakov A & Kurbatov R, *Russ J Inorg Chem*, 52 (2007) 1971.
28 Khor S, Talib Z & Yunus W M, *Ceram Int*, 38 (2012) 935.
29 Lim T Y, Wagiran H, Hussin R, Hashim S & Saeed M, *Physica B Condens Matter*, 451 (2014) 63.
30 Mugoni C, Gatto C, Pla-Dalmau A & Siligardi C, *J Non-Cryst Solids*, 471 (2017) 295.
31 Berkemeier F, Voss S, Imre Á W & Mehrer H, *J Non-Cryst Solids*, 351 (2005) 3816.
32 López R & Gómez R, *J Solgel Sci Technol*, 61 (2012) 1.
33 Mortazavi-Derazkola S, Zinatloo-Ajabshir S & Salavati-Niasari M, *J Mater Sci: Mater Electron*, 26 (2015) 5658.
34 Kubelka P & Munk F, *Z Tech Phys*, 12 (1931) 259.
35 Kubelka P, *J Opt Soc Am*, 38 (1948) 448.
36 Abd El-Moneim A, *Mater Chem Phys*, 52 (1998) 36.
37 Abd El-Moneim A, Youssof I & Abd El-Latif L, *Acta Mater*, 54 (2006) 3811.
38 Sidkey M, Abd El-Moneim A, Gaafar M, Abd El-Aal N, Abd El-Latif L & Youssof I, *Philos Mag Lett*, 88 (2008) 1705.
39 Alajerami Y S M, Hashim S, Hassan W M S W & Ramli A T, *Physica B Condens Matter*, 407 (2012) 2390.
40 Ichoja A, Hashim S, Ghoshal S, Hashim I & Omar R, *J Rare Earths*, 36 (2018) 1264.
41 Prabhu N S, Hegde V, Wagh A, Sayyed M, Agar O & Kamath S D, *J Non-Cryst Solids*, 515 (2019) 116.
42 Arya S, Kaur G & Singh K, *J Non-Cryst Solids*, 432 (2016) 393.
43 Kim D, Kim W, Park E, Mattern N & Eckert J, *Prog Mater Sci*, 58 (2013) 1103.
44 Phillips G, A concise introduction to ceramics (Springer Science & Business Media, New York), 2012, p. 12.
45 Ramteke D & Gedam R, *Spectrosc Lett*, 48 (2015) 417.
46 Pawar P, Munishwar S & Gedam R, *J Alloys Compd*, 660 (2016) 347.
47 Jayasimhadri M, Jang K, Lee H S, Chen B, Yi S-S & Jeong J H, *J Appl Phys*, 106 (2009) 013105.
48 Nawaz F, Sahar M R, Ghoshal S, Amjad R J, Dousti M & Awang A, *Chin Opt Lett*, 11 (2013) 061605.
49 Kaur R, Rakesh R, Mhatre S G, Bhatia V, Kumar D, Singh H, Singh S P & Kumar A, *Opt Mater*, 117 (2021) 111109.
50 Kitis G, Gomez-Ros J & Tuyn J W, *J Phys D: Appl Phys*, 31 (1998) 2636.
51 Puchalska M & Bilski P, *Radiat Meas*, 41 (2006) 659.
52 Salama E & Soliman H, *Radiat Phys Chem*, 148 (2018) 95.

53 Balian H G & Eddy N W, *Nucl Instrum Methods*, 145 (1977) 389.

54 Salah N, Sahare P, Nawaz S & Lochab S, *Radiat Eff Defects Solids*, 159 (2004) 321.

55 Bossin L, Kazakis N A, Kitis G & Tsirliganis N C, *Appl Radiat Isot*, 127 (2017) 26.

56 Gómez-Ros J M, Correcher V, García-Guinea J & Delgado A, *Radiat Prot Dosim*, 100 (2002) 399.

57 Azizan S, Hashim S, Razak N, Mhareb M, Alajerami Y & Tamchek N, *J Mol Struct*, 1076 (2014) 20.

58 Lakshminarayana G, Kaky K M, Baki S, Lira A, Nayar P, Kityk I & Mahdi M, *J Alloys Compd*, 690 (2017) 799.

59 Edukondalu A, Kavitha B, Samee M, Ahmmed S K, Rahman S & Kumar K S, *J Alloys Compd*, 552 (2013) 157.

60 Edukondalu A, Srinivasu C, Rahman S & Kumar K, *Int J Sci Eng*, 5 (2014) 258.

61 Verhoef A & Den H H, *J Non-Cryst Solids*, 182 (1995) 235.

62 Verhoef A & Den H H, *J Non-Cryst Solids*, 182 (1995) 221.

63 Gautam C, Yadav A K & Singh A K, *Int Sch Res Notices*, 2012 (2012).

64 Kaky K M, Lakshminarayana G, Baki S, Taufiq-Yap Y, Kityk I & Mahdi M, *J Non-Cryst Solids*, 456 (2017) 55.